scientific reports

Check for updates

OPEN

Transcriptomic comparison of corneal endothelial cells in young versus old corneas

Jin Sun Hwang[1,2,4], Je Hyun Seo[3,4], Hyeon Jung Kim[1,2], Yunkyoung Ryu[1,2], Young Lee[3] & Young Joo Shin[1,2]✉

Corneal endothelial cells, situated on the innermost layer of the cornea, are vital for maintaining its clarity and thickness by regulating fluid. In this study, we investigated the differences in the transcriptome between young and old corneal endothelial cells using next-generation sequencing (NGS). Cultured endothelial cells from both young and elderly donors were subjected to NGS to unravel the transcriptomic landscape. Subsequent analyses, facilitated by Metascape, allowed for the dissection of gene expression variances, unearthing pivotal biological pathways. A total of 568 genes showed differences, and were related to Endomembrane system organization, nuclear receptors meta pathway, efferocytosis, etc. Notably, a reduction in the expression of 260 genes was observed in the aged cells form old donors, and in the related analysis, eukaryotic translation initiation, integrator complex, and Hippo YAP signaling were significant. Conversely, 308 genes exhibited elevated expression levels in the elderly, correlating with processes including transition metal ion transport and glycoprotein biosynthesis. In conclusion, our investigation has revealed critical genes involved in the aging process of corneal endothelial cells and elucidated their underlying biological pathways. These insights are instrumental in selecting targets for therapeutic intervention, thereby facilitating the advancement of novel therapeutic approaches for the restoration and preservation of corneal endothelial cell function.

Corneal endothelial cells, residing in the innermost layer of the cornea, are vital for maintaining its clarity and thickness through fluid regulation[1]. Severe damage to these cells leads to corneal blindness or bullous keratopathy requiring corneal transplantation, because corneal endothelial cells have very limited regenerative abilities in vivo[2]. The mechanisms by which corneal endothelial cells fail to regenerate has been reported to include cell cycle arrest, abundant negative cytokine in anterior chamber, and senescence[3]. Senescence is a hallmark of aging process, playing a crucial role in both the biological aging of organisms and the development of age-related diseases[4], and is similar to in vivo wound healing of corneal endothelial cells in that cells do not proliferate and are enlarged[5]. Thus, understanding the differences between the corneal endothelial cells of the young and the old is important for pioneering future therapeutic strategies for corneal endothelial regeneration. Differences in corneal endothelial cells between old and young donors have been reported, including proliferative capacity, cell cycle dynamics and protein expression[6–9]. This study employed next-generation sequencing (NGS) to analyze the transcriptome differences between young and old corneas. NGS represents an array of advanced sequencing technologies designed for fast, high-throughput analysis of DNA and RNA sequences[10]. Gene expression analysis involves quantifying the levels of mRNA produced from genes in a cell, providing insights into the functional state of those cells[10]. This comparison could reveal significant insights into gene expression changes, regulatory mechanisms, and pathways that are influenced by aging[11]. In this study, we investigated the differences in the transcriptome of corneal endothelial cells between young and old corneas using NGS, thereby elucidating the regulatory mechanisms and pathways influenced by aging.

Methods

This study was performed in accordance with the tenets of the Declaration of Helsinki and was reviewed and approved by the institutional review board/ethics committee (IRB) of the Hallym University Medical Center.

[1]Department of Ophthalmology, Hallym University College of Medicine, Hallym University Medical Center, 1 Shingil-ro, Youngdeungpo-gu, Seoul 07441, Korea. [2]Hallym BioEyeTech Research Center, Hallym University College of Medicine, Seoul, Republic of Korea. [3]Veterans Health Service Medical Center, Veterans Medical Research Institute, Seoul, Republic of Korea. [4]Jin Sun Hwang and Je Hyun Seo have contribute equally to this work. ✉email: schinn@hanmail.net

Cells were cultured according to previously published methods[12]. Corneas were purchased from Eversight (Ann Arbor, MI), which had obtained informed consents for donated corneas. Because it was practically impossible to obtain consent from research subjects or human material donors in the case of human material research during the research process, the consent form was waived by the institutional review board/ethics committee of the Hallym University Medical Center. Corneas from three donors in each group were used. Human corneal endothelial cells-Descemet's membrane complex was incubated for 10 min in 0.25% trypsin/0.02% ethylenediaminetetraacetic acid (EDTA) solution. Cells were then plated in 6-well plates coated with a fibronectin–collagen combination (FNC) coating mix (Athena Environmental Sciences, Inc., Baltimore, MD, USA). Cells were cultured to confluence for 10–14 days and then passaged at a ratio of 1:3 using 0.25% trypsin/0.02% EDTA solution. Donor ages were 26.6 ± 6.2y in young cornea ($n = 5$) and 69.3 ± 9.0y in old corneas ($n = 4$).

Cell shape evaluation and immunofluorescence staining

Cell shape was evaluated and microscopic images were obtained using an inverted fluorescence microscope (DMi8, Leica, Wetzlar, Germany). Immunofluorescence of ZO-1 was performed. Samples were initially rinsed with phosphate-buffered saline (PBS) and subsequently fixed in a 4% paraformaldehyde solution for 20 min. Permeabilization was performed with a 0.5% Triton X-100 solution for 10 min, followed by a blocking step with 1% bovine serum albumin (BSA) at 25 °C for one hour. Overnight incubation at 4 °C was performed with one of several antibodies: rat anti-ZO-1 (sc-33725, Santa Cruz Biotechnology, Santa Cruz, CA, USA). After washing with PBS, samples were incubated with fluorescein isothiocyanate (FITC)-conjugated goat anti-rat IgG (1:100) for 2 h at 25 °C in darkness, followed by counterstaining with Hoechst 33,342 nuclear staining dye (1:2000; Molecular Probes, Eugene, OR, USA). Observations were made using a fluorescence microscope (DMi8), and images were documented.

Transcriptome analysis and Analysis of differentially expressed genes (DEGs) and functional analyses of DEGs

RNA extraction was meticulously conducted using the ReliaPrep™ RNA Miniprep Systems (Promega, Madison, WI, USA), ensuring the retrieval of high-quality RNA for further analysis. The sequencing of the extracted RNA was performed at MacroGen Inc. (www.macrogen.com), utilizing the advanced Illumina HiSeq 2000 platform[13]. This high-throughput sequencing technology facilitated a comprehensive examination of the transcriptome, enabling precise quantification and identification of gene expression differences across samples. For the analysis of differentially expressed genes (DEGs), the edgeR package and R 3.6.3 program (R Foundation, Vienna, Austria) were employed, a robust statistical tool designed for examining RNA sequencing data[14]. DEGs were identified based on stringent criteria: a $\log_2$(fold change (FC)) ≥ 1 combined with a false discovery rate (FDR) of < 0.05, ensuring that only statistically significant alterations in gene expression were considered. StringTie version 1.3.4d and DESeq2 software were used to calculate transcript abundances and confirm DEGs between young and old corneal endothelial cells[15,16]. The calculation of transcript abundances was performed using the Fragments Per Kilobase of transcript per Million mapped reads (FPKM) metric, providing a normalized measure of gene expression levels. To address the multiple comparison problem and reduce the likelihood of type I errors, FDR control was meticulously applied using the Benjamini–Hochberg algorithm, adjusting p-values to more accurately reflect the discovery of true positives.

Functional annotation and network analysis were performed using a Kyoto Encyclopedia of Genes and Genomes (www.kegg.jp/kegg/kegg1.html) or Metascape (https://metascape.org/gp/index.html#/main/step1), which was employed for the identification of metabolic pathways or signal transduction pathways that were significantly enriched in DEGs[17]. In addition, STRING database (https://string-db.org/) and ShinyGO0.80 were used for network analysis and functional annotation. GO terms and pathways with an adjusted p-value < 0.05 were considered significantly enriched.

Function and pathway enrichment analysis

Metascape (http://metascape.org/gp/index.html#/main/step1)[18] serves as a sophisticated tool for gene function annotation, leveraging advanced bioinformatics methodologies for the batch analysis of genes and proteins to elucidate their biological functions. It offers researchers the capability to annotate an extensive array of genes or proteins comprehensively, facilitating the exploration of their roles within biological contexts. Furthermore, Metascape enables the performance of enrichment analysis, a crucial step in interpreting large-scale genomics and proteomics data by identifying over-represented functional categories that may shed light on the underlying biological processes. Additionally, the construction of protein–protein interaction (PPI) networks through Metascape provides invaluable insights into the molecular interactions and signaling pathways, allowing for a deeper understanding of cellular mechanisms. This multifaceted approach not only streamlines the functional analysis of gene sets but also significantly enhances the ability to uncover novel insights into the complex dynamics of biological systems[19].

Results

Cell shape and DEGs

The morphology of corneal endothelial cells from young and old donors was evaluated to gain the insight into the health of cells (Fig. 1A). Compared to young cells, old corneal endothelial cells were larger. Immunofluorescence staining of ZO-1 showed the distribution of the ZO-1 protein within cells (Fig. 1B). ZO-1 is a key protein found in tight junctions, which are structures that tightly seal cells together in corneal endothelial cells, creating a barrier and controlling the passage of molecules. ZO-1 appeared as continuous lines at the cell borders, outlining where cells meet and form junctions. We selected all significantly up-regulated and down-regulated mRNAs in corneal endothelial old donor to plot their expression on principal component analysis (PCA) plot, heat-maps

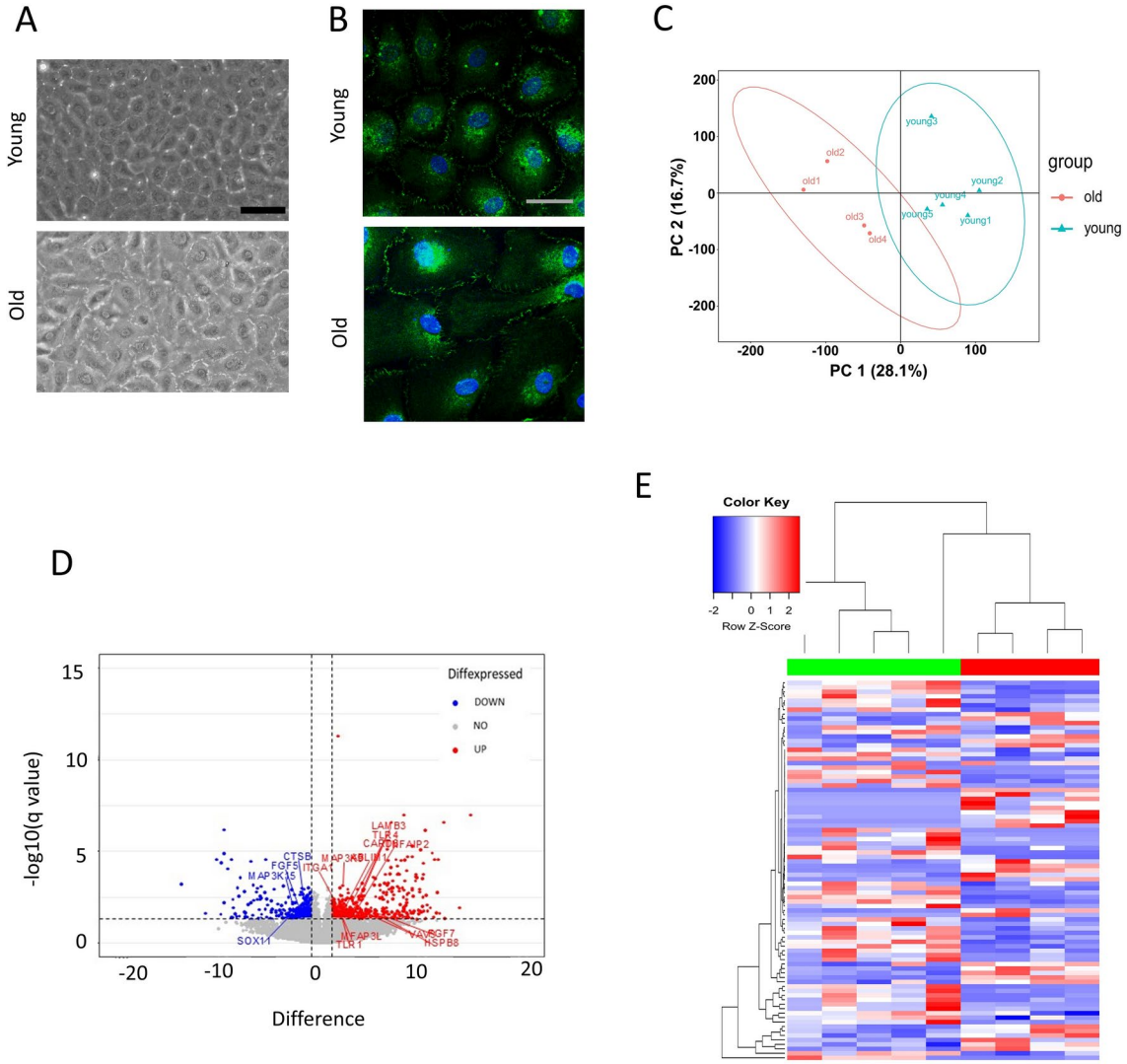

Fig. 1. (**A**) Morphology of corneal endothelial cells from young and old donor. Scale bar = 100 µm. (**B**) Immunofluorescence staining of ZO-1 was performed. Scale bar = 25 µm. (**C**) Principal component analysis (PCA) plot, (**D**) Volcano plot, (**E**) Heatmap of differentially expressed mRNAs from corneal endothelial cells from young and old donor.

and volcano plots of differentially expressed mRNAs (Fig. 1C-1E). The significantly up-regulated and down-regulated DEGs are shown in Tables 1. The NGS analysis resulted in the identification of 568 DEGs. Of this total, 308 were characterized by upregulation and 260 by downregulation in corneal endothelial cells from older donors. These DEGs underwent further examination through the ShinyGO 0.80 (http://bioinformatics.sdstate.edu/go/) and the Metascape tool (http://metascape.org/gp/index.html#/main/step1).

Enrichment analysis of total differentially expressed genes

Functional enrichment analysis, conducted via Metascape, revealed that DEGs between young and old corneal endothelial cells were markedly enriched in several biological processes. These processes include endomembrane system organization, the nuclear receptors meta pathway, efferocytosis, and the positive regulation of cellular component biogenesis. Additionally, significant enrichment was observed in the cellular response to abiotic stimuli, positive regulation of aspartic-type endopeptidase activity—which plays a critical role in the amyloid precursor protein catabolic process—proteoglycan biosynthesis, positive regulation of stress fiber assembly, and peroxisomal membrane transport ($p < 0.05$; see Fig. 2 and Table 2).

The enrichment analysis of PPI among the total DEGs is presented in Table 3 and Fig. 3. The MCODE plugin, a tool designed for the identification of functional modules within PPI networks, was employed for this analysis. Top-scored modules were translation, eukaryotic translation elongation, nonsense mediated decay (NMD) independent of the exon junction complex (EJC), RMTs methylate histone arginines, diseases of programmed cell death, heterochromatin organization, Golgi associated vesicle biogenesis, trans-Golgi network vesicle budding, membrane trafficking, COPI-mediated anterograde transport, ER to Golgi anterograde transport, transport to

Gene	P value	q value
Up-regulated		
SGSM3	0.000808	0.045453
SUPT7L	0.000805	0.045448
DGCR6L	0.000343	0.035461
TIMM29	0.000567	0.040427
KDELR1	0.000036	0.01458
SHOC2	< 0.000001	0.002559
IPO13	0.000054	0.016326
ZSCAN18	0.000226	0.03223
BET1L	0.000404	0.036897
EXOC6B	0.000108	0.0238
FAM222B	0.000284	0.033477
STAT2	0.00019	0.03021
SLC39A9	0.000049	0.015769
ZBTB47	0.000497	0.039341
S100A11	0.00054	0.039993
ATP6AP2	0.000442	0.037836
TMEM219	0.000342	0.035461
SEC16A	0.001104	0.049351
ITGAE	0.000666	0.041674
TESK1	0.001066	0.048858
SELENOW	0.000914	0.046274
TAX1BP1	0.00107	0.048874
B4GALT3	0.000595	0.040784
ROCK1P1	0.000895	0.045822
ZDHHC9	0.000457	0.038152
TOR1AIP2	0.000286	0.033477
TMED7	0.000803	0.045448
AP1B1	0.000046	0.015333
SLC39A7	0.000982	0.047339
SCYL1	0.00058	0.040704
ZNF275	0.000182	0.029422
POMT1	0.000836	0.045574
FBXL7	0.00078	0.044762
SLC4A2	0.000044	0.015295
PRDX2	0.000029	0.012822
NBPF3	0.000089	0.021595
PPP1R12A-AS1	0.000245	0.032923
MINPP1	0.000688	0.042365
ATXN10	0.00054	0.039993
CPD	0.001026	0.047944
PKP4	0.000364	0.035865
SLC30A7	0.001095	0.049199
PIP5K1C	0.000075	0.019397
MICOS10	0.000227	0.03223
EMC10	0.000156	0.028623
YIPF2	0.000448	0.038084
TCTN3	0.000215	0.031763
ABHD15	0.000761	0.044109
PXN	0.000108	0.0238
BDH2	0.000013	0.008443
KIAA2013	0.00093	0.046401
SDF4	0.000173	0.029412
TBC1D12	0.000543	0.039993
THEM4	0.001016	0.047924
ZSCAN16-AS1	0.000008	0.007177
Continued		

Gene	P value	q value
MYDGF	0.000631	0.041521
SLC35B3	0.000351	0.035587
DEXI	0.000626	0.041267
C12orf73	0.000546	0.039993
SLC35E1	0.00029	0.033477
RNF121	0.001018	0.047924
SLC39A11	0.00036	0.035721
ATP6AP1	0.000358	0.035721
MGAT2	0.000588	0.040704
ATP1B3	0.00065	0.041674
DNAJC15	0.000526	0.039977
DNASE2	0.000472	0.038402
ZC3H12B	0.000608	0.040872
PGRMC2	0.000077	0.019618
EVI5	0.000643	0.041674
ZFYVE27	0.000589	0.040704
B3GAT3	0.000185	0.029654
MFSD12	0.001068	0.048858
ALG11	0.000589	0.040704
AFF1	0.000195	0.030564
PGAP6	0.000136	0.02705
GLS	0.000896	0.045822
ENG	0.000324	0.035114
RNU6-3P	0.000337	0.035461
P3H4	0.00109	0.049199
WIPI1	0.000495	0.039341
BTBD3	0.000044	0.015295
TPR	0.000865	0.045651
SLC38A10	0.000212	0.031713
SEZ6L2	0.001108	0.049366
ABCD3	0.001115	0.049496
RNASET2	0.00066	0.041674
PBLD	0.000067	0.017747
TCTA	0.000446	0.037982
BMPR1B	0.000246	0.032923
PICALM	0.000227	0.03223
LOC101927365	0.000667	0.041674
H2AJ	0.00005	0.015769
DYNLL2	0.001052	0.048783
ERN1	0.001085	0.049199
ATP2C1	0.000441	0.037836
RNU6-1	0.000704	0.042803
TECTA	0.000829	0.045574
SMPD1	0.000179	0.029422
NUAK1	0.000254	0.032923
EMC1-AS1	0.000528	0.039977
ARHGEF5	0.000137	0.02705
LONP2	0.000122	0.02551
SLC41A2	0.000196	0.030564
IER3-AS1	0.000209	0.031713
HTRA1	0.000997	0.047567
CHPF	0.000312	0.034655
CHST3	0.000124	0.025547
TGFB1	0.000517	0.039977
GPR157	0.000037	0.014924
SLC5A10	0.001006	0.047889
Continued		

Gene	P value	q value
NPIPB15	0.000434	0.037836
RNU6-36P	0.000177	0.029412
ENTPD7	0.000945	0.046804
GADD45B	0.000214	0.031713
SNORA14B	0.000871	0.045651
PPP1R13B	0.001138	0.049979
ARHGEF34P	0.000537	0.039993
MAPK13	0.000658	0.041674
CKAP4	0.000439	0.037836
SCARB1	0.000961	0.047339
PLA2G15	0.001144	0.049979
SLC22A23	0.001134	0.049958
PAPSS2	0.000301	0.034253
CFHR1	0.000848	0.045574
MIR770	< 0.000001	0.000005
GSTT2B	0.000001	0.002777
MFSD6	0.000854	0.045643
SIRPA	0.000849	0.045574
IRF5	0.000107	0.0238
ARHGEF35	0.000108	0.0238
FBN1	0.000985	0.047339
IER3	0.000182	0.029422
CSRNP1	0.000617	0.041144
VEGFC	0.00006	0.017196
CYB561	0.000327	0.035225
PODXL2	0.000335	0.035461
MR1	0.000834	0.045574
WDR66	0.000981	0.047339
DOK1	0.000007	0.007148
IGFBP7	0.000709	0.042809
GRAMD2B	0.000207	0.031713
SLC46A3	0.000761	0.044109
DOCK9-DT	0.000659	0.041674
SLC16A2	0.000526	0.039977
SEMA3C	0.000966	0.047339
GSTT2	< 0.000001	0.002036
ANO5	0.000985	0.047339
BNC2-AS1	0.000261	0.032923
ABAT	0.000774	0.044592
GATA2-AS1	0.001099	0.049199
CFH	0.000608	0.040872
GALNT5	0.000283	0.033477
KBTBD8	0.000879	0.045667
MAP3K9	0.000007	0.007177
MID2	0.000727	0.043521
TMEM255B	0.000171	0.029406
REPS2	0.00102	0.047924
H1-4	0.000026	0.012261
H2AC6	0.000594	0.040784
ABLIM1	0.000289	0.033477
SGK1	0.000623	0.041267
EPHX2	0.000381	0.036676
OXCT2P1	0.00062	0.041256
ZNF365	0.000032	0.013726
USP32P2	0.000082	0.020537
CD55	0.000597	0.040797
Continued		

Gene	P value	q value
PCDHGA4	0.000884	0.045777
KCTD16	0.000742	0.043844
MEGF10	0.000993	0.047471
KCNK1	0.000436	0.037836
RNF180	0.000554	0.040233
PRKG2	0.000874	0.045651
NFASC	0.000218	0.031852
TLR4	0.000403	0.036897
PMEPA1	0.000692	0.042369
SLC4A11	0.000538	0.039993
PLEKHH1	0.00032	0.034952
KCNT2	0.000887	0.045818
SLC22A15	0.000101	0.023385
PDZD2	0.00016	0.028639
ACSL5	0.000502	0.039341
RGS4	0.000432	0.037836
H4C8	0.00105	0.048783
LINC01138	0.000372	0.036369
ANKRD6	0.000332	0.035296
GPRC5D-AS1	0.000008	0.007177
ACOT11	0.000352	0.035587
HSPA12A	0.000049	0.015769
TPD52	0.000554	0.040233
TMEM233	0.000267	0.032923
ADAMTS5	0.000993	0.047471
ZBED2	0.000485	0.039158
NEDD9	0.000043	0.015295
CES4A	0.000063	0.017352
GPRC5B	0.001098	0.049199
CNTNAP3	0.000352	0.035587
HERC2P7	0.000039	0.015132
TRPM3	0.000913	0.046274
APOL1	0.000467	0.038324
WSCD1	0.000193	0.030515
GALNT18	0.000462	0.038321
POLRMTP1	0.000331	0.035296
TMEM229B	0.000896	0.045822
TENM2	0.000737	0.0437
LARGE1	0.000098	0.022834
FGF7	0.000406	0.036897
SLC2A3P2	0.000059	0.017107
CNTNAP3P2	0.00009	0.021772
GBP4	0.000001	0.002571
BEND7	0.000848	0.045574
CHST15	0.000217	0.031852
RNASEH1P2	0.000415	0.037188
PTGFRN	0.000051	0.015769
MX2	0.001041	0.048539
HTR1D	0.000287	0.033477
MPZL3	0.000012	0.008443
PAX8-AS1	0.000129	0.026371
DIO2	0.000556	0.040233
LINC00639	0.00052	0.039977
WDR93	0.000067	0.017747
SMOC1	0.000331	0.035296
CNTNAP3B	0.000023	0.011409
Continued		

Gene	P value	q value
LOC101929268	0.000258	0.032923
RPS10P1	0.000993	0.047471
SAMD9	0.00017	0.029406
IL21-AS1	0.000637	0.041674
GAS2L1P2	0.00008	0.020215
JPH2	0.000317	0.034952
COL10A1	0.000965	0.047339
TTBK1	0.000698	0.042626
LINC01235	0.000004	0.006366
P4HA3-AS1	0.000045	0.015295
OR2S2	0.000058	0.017015
CYP51A1P1	0.000115	0.024852
MYBPC1	0.000012	0.008443
OGFR-AS1	0.001107	0.049366
LINC00511	0.000397	0.036897
IQCA1	0.000868	0.045651
LINC02542	< 0.000001	0.001529
ERMN	0.00002	0.010222
ANGPTL7	0.000244	0.032923
TPTE2	0.000118	0.024907
PDE6A	0.000143	0.027256
MESTIT1	0.000132	0.026713
TECTB	0.000397	0.036897
LOC105373553	0.000083	0.02069
UBE2QL1	0.000282	0.033477
MYRFL	0.000176	0.029412
LINC00856	0.000006	0.007148
CCN4	0.000013	0.008443
GPR68	0.000342	0.035461
CXADRP3	0.000087	0.021254
LIMCH1	0.000024	0.011594
LINC02613	0.000024	0.011594
GPAT2P1	0.000235	0.032746
CD1D	0.000028	0.012309
LINC01592	0.000044	0.015295
C8orf34-AS1	0.000377	0.036426
VWA2	0.00001	0.007485
RNU5E-1	0.000687	0.042365
CDH10	0.000309	0.034574
RSPO4	0.00026	0.032923
FOXO6	0.000013	0.008443
ARMC4	0.001097	0.049199
H2AC21	< 0.000001	0.001303
TSPEAR-AS1	0.000679	0.042008
FGF16	0.00002	0.010222
FAM95C	0.00022	0.031852
LOC100132057	0.000018	0.009982
ADGRF4	0.000964	0.047339
MIR412	0.000278	0.033477
EGLN3	0.000571	0.040459
SNORD114-13	0.000009	0.007271
CYP24A1	0.000204	0.031489
HLA-V	0.000562	0.040404
FGFR2	0.000159	0.028639
LINC02575	0.000005	0.00691
CNTNAP3P4	0.000002	0.00346
Continued		

Gene	P value	q value
FBP1	0.000248	0.032923
KRTAP5-AS1	0.000925	0.046274
NYAP2	0.000415	0.037188
MAPK4	0.000865	0.045651
LINC01561	0.000406	0.036897
VIT	0.000047	0.01558
FAM201A	0.000027	0.012267
TRBJ2-1	0.000033	0.013816
MIR369	0.000039	0.015132
IDO1	0.000454	0.038152
GPAT2	0.000063	0.017352
LINC01239	0.00014	0.02705
SLC37A1	0.000781	0.044762
SMCO3	0.000662	0.041674
KLHL4	0.000004	0.006425
DHRS2	0.000011	0.008198
SPINK1	0.00004	0.015132
ADORA1	0.001127	0.049814
ENTPD3	< 0.000001	0.002024
DLX5	0.000354	0.035587
PTPN20	0.000163	0.028856
CECR7	0.001139	0.049979
SNORD113-3	0.000004	0.006366
CGA	0.000009	0.007271
TDRD1	0.000016	0.009926
PIEZO2	0.000919	0.046274
BEX1	0.000257	0.032923
MEG9	< 0.000001	0.001584
PSPHP1	< 0.000001	0.001303
Down-regulated		
SPOCK3	0.000064	0.017352
LINC00491	0.000006	0.007148
CDIPTOSP	0.000009	0.007271
LINC01925	0.000003	0.005406
CDKL4	< 0.000001	0.001584
GABRA4	0.000547	0.039993
LLPH-DT	0.000016	0.009643
GNG3	0.000006	0.007148
CDK2AP2P1	0.000384	0.03677
RPL36AP15	0.000097	0.022834
HCG22	0.000266	0.032923
NPFFR2	0.000035	0.01458
TBX4	0.001112	0.049443
MLLT10P1	0.000156	0.028623
SGCZ	0.00073	0.043558
SFRP1	0.001143	0.049979
FAUP1	0.000008	0.007177
RPS25P2	0.000564	0.040404
RSL24D1P11	0.000073	0.018976
FAM225A	0.000442	0.037836
RPS4XP22	0.000164	0.028909
GABRB1	0.000117	0.024907
FAM225B	0.000387	0.03686
RPS7P3	0.000404	0.036897
TP53TG3B	0.000263	0.032923
TP53TG3C	0.00032	0.034952
Continued		

Gene	P value	q value
EMILIN3	0.001012	0.047924
USP32P1	0.000289	0.033477
DBF4P1	0.00017	0.029406
HTATSF1P2	0.000007	0.007148
KCNN2	0.000376	0.036426
TP53TG3	0.00037	0.036319
BCHE	0.000667	0.041674
RPS2P7	0.000286	0.033477
RPS2P20	0.000648	0.041674
LY6K	0.000658	0.041674
CCDC144A	0.000306	0.034464
TPPP3	0.00087	0.045651
PCDHGA11	0.000267	0.032923
LOC100288175	0.000296	0.033862
APLN	0.000556	0.040233
LOC440568	0.000239	0.032923
LRRCC1	0.000817	0.045535
MAMDC2	0.000309	0.034574
APOBEC3D	0.000514	0.039977
SSC5D	0.000044	0.015295
WDR17	0.000131	0.026551
ZNF560	0.000657	0.041674
SNORD135	0.00042	0.037192
USP44	0.000736	0.0437
LINC01140	0.000304	0.034464
NR1H3	0.000051	0.015769
PGGHG	0.000806	0.045448
DDIT4	0.000559	0.040315
MNS1	0.000648	0.041674
DPYSL2	0.000758	0.044109
AOC3	0.000812	0.045484
CGAS	0.000027	0.012261
SNCA	0.00098	0.047339
RPS2P55	0.000601	0.040865
MYO15B	0.000918	0.046274
EIF4EBP1	0.00023	0.03223
CEBPD	0.000799	0.045357
RAPGEF4	0.000546	0.039993
A2M-AS1	0.001065	0.048858
RPL23AP87	0.000625	0.041267
RPL9P8	0.000835	0.045574
POU2F2	0.000242	0.032923
FAM161A	0.000063	0.017352
GOLGA8H	0.000438	0.037836
IL7	0.000672	0.041899
ARL6IP6	0.000604	0.040872
CDCA4	0.000974	0.047339
ARNTL2	0.000093	0.022161
THAP9-AS1	0.000641	0.041674
RPL23AP4	0.000866	0.045651
B3GNT5	0.000455	0.038152
CHRAC1	0.00026	0.032923
VEGFA	0.000757	0.044109
SIAH1	0.000879	0.045667
PTPRG-AS1	0.001141	0.049979
SKAP2	0.000174	0.029412
Continued		

Gene	P value	q value
PSD3	0.000118	0.024907
SLCO3A1	0.000985	0.047339
MST1	0.000343	0.035461
RPS2P5	0.000757	0.044109
KIAA1324	0.000354	0.035587
EIF3E	0.000608	0.040872
LONRF1	0.000527	0.039977
TCEA1	0.000493	0.039341
ATP23	0.001019	0.047924
KIFC2	0.000586	0.040704
MED30	0.000323	0.035095
RPL7	0.000874	0.045651
PPP1R3B	0.000407	0.036897
ZFP69B	0.000797	0.045349
PLAG1	0.000285	0.033477
RN7SL832P	0.000212	0.031713
EFNA3	0.000653	0.041674
AMZ2P1	0.00011	0.023831
CENPP	0.000936	0.046543
NECTIN3	0.000657	0.041674
FMNL2	0.000757	0.044109
TBPL1	0.000144	0.027256
AGER	0.000103	0.023571
BNIP3L	0.000791	0.045171
LOXL2	0.000183	0.029422
DCLRE1B	0.000611	0.040872
NCOA2	0.000455	0.038152
RPS2P46	0.000834	0.045574
WHAMMP1	0.00027	0.033189
SAV1	0.00112	0.049594
STK17B	0.000543	0.039993
CUL7	0.001026	0.047944
NSMCE2	0.000211	0.031713
TRAF3IP2-AS1	0.000856	0.045651
STK3	0.000019	0.010222
RPL23AP79	0.001059	0.048858
RBIS	0.000058	0.017015
RPL30	0.000587	0.040704
RPS20	0.000376	0.036426
RPS27P3	0.000145	0.027256
INTS8	0.0004	0.036897
FAM86B3P	0.000834	0.045574
PPM1M	0.000566	0.040426
SNX16	0.000013	0.008443
PABPC1	0.000107	0.0238
VPS13B	0.000293	0.033638
SLC66A1L	0.000496	0.039341
SPIDR	0.00069	0.042367
POLG2	0.000278	0.033477
GASAL1	0.000874	0.045651
ASH2L	0.00042	0.037192
RPL29P11	0.000494	0.039341
RPS3AP5	0.000253	0.032923
TMEM256	0.000953	0.047083
MRPL13	0.000709	0.042809
DNALI1	0.000025	0.012148
Continued		

Gene	P value	q value
DPH6	0.001134	0.049958
DUS4L	0.000045	0.015295
ENY2	0.001066	0.048858
AFDN	0.000141	0.02705
LRRC37A2	0.000178	0.029412
ZNF623	0.000839	0.045574
DHRS4-AS1	0.000409	0.036932
ZNF706	0.000649	0.041674
CAMK2D	0.00101	0.047924
C11orf54	0.001061	0.048858
SNHG29	0.000244	0.032923
NEO1	0.000775	0.044592
ARHGEF10	0.000472	0.038402
HMGN1P18	0.000916	0.046274
FAM66B	0.000265	0.032923
PGBD1	0.000339	0.035461
AP1S2	0.000907	0.046274
ANP32B	0.000064	0.017352
NLN	0.000468	0.038324
WRN	0.000149	0.02771
ERICH1	0.000229	0.03223
WASHC5	0.0006	0.040865
SINHCAF	0.001017	0.047924
ATF1	0.001065	0.048858
ZFAND1	0.000263	0.032923
HILPDA	0.001052	0.048783
TPT1	0.000006	0.007148
UBXN2B	0.000314	0.034792
LRRC37A	0.000056	0.01668
IQCH	0.000459	0.038228
PABPC5	0.000676	0.041996
PBX2P1	0.000727	0.043521
NSD3	0.00036	0.035721
STARD3NL	0.000468	0.038324
SMIM19	0.000914	0.046274
RPS15A	0.000761	0.044109
TRIQK	0.000826	0.045574
ALPK1	0.000506	0.03944
CACYBP	0.000362	0.035727
ARHGAP21	0.000229	0.03223
EMC2	0.0004	0.036897
WASHC1	0.000043	0.015295
ZNF251	0.000924	0.046274
PRSS53	0.000569	0.040427
SLC2A1	0.00054	0.039993
EEF1D	0.000738	0.0437
CCDC25	0.000002	0.003769
INTS10	0.001084	0.049199
XPO7	0.000634	0.041617
VDAC3	0.000477	0.038633
AASDH	0.000976	0.047339
ARHGAP4	0.000388	0.03686
GARS-DT	0.000792	0.045171
RPL27A	0.00061	0.040872
MAGOHB	0.000176	0.029412
PPP1R12B	0.001085	0.049199
Continued		

Gene	P value	q value
PLEC	0.00109	0.049199
ZFP41	0.000853	0.045643
ZNF558	0.000204	0.031489
RESF1	0.000647	0.041674
PTGES3	0.000159	0.028639
DDHD2	0.000018	0.009982
DDAH2	0.000722	0.043475
MYL5	0.000942	0.046727
MORC3	0.000518	0.039977
SPTSSA	0.000584	0.040704
PACRGL	0.000499	0.039341
R3HDM4	0.000465	0.038324
PEX2	0.000529	0.039977
SRXN1	0.000018	0.009982
FAM193B	0.000018	0.009982
ZNF333	0.000051	0.015769
TRNAU1AP	0.000139	0.02705
ACAP3	0.000935	0.046543
ATXN2L	0.00109	0.049199
CRYZL1	0.000925	0.046274
ADAT2	0.00081	0.045458
TRMT12	0.000924	0.046274
FXR1	0.0005	0.039341
C2orf74	0.000408	0.036897
CAB39	0.000821	0.045574
LYST	0.000728	0.043521
ZSWIM7	0.000503	0.039341
AFMID	0.000436	0.037836
ZSCAN26	0.000288	0.033477
BIN3	0.000847	0.045574
ZNF397	0.000395	0.036897
IFT88	0.00016	0.028639
PUF60	0.000832	0.045574
SLC25A43	0.000842	0.045574
YWHAZ	0.000861	0.045651
MOCS2	0.000454	0.038152
PIP4P2	0.000985	0.047339
SFXN3	0.000749	0.044109
ATPSCKMT	0.001093	0.049199
COG4	0.000763	0.044109
TAF15	0.000138	0.02705
ERLIN2	0.000242	0.032923
RAB2A	0.000894	0.045822
PI4KAP1	0.00088	0.045667
PARP4	0.000703	0.042803
FNTA	0.001023	0.047944
ABCD4	0.000261	0.032923
RHBDD1	0.000417	0.037192
TBXAS1	0.000392	0.036897
FBXO38	0.000345	0.035538
SRSF4	0.000579	0.040704
RNF139	0.000421	0.037192
RNF214	0.000709	0.042809
UBA3	0.000258	0.032923
INTS11	0.000825	0.045574
SPRED2	0.000582	0.040704
Continued		

Gene	P value	q value
GNPAT	0.000592	0.040784
JRKL	0.000502	0.039341
RBMS1	0.000985	0.047339
TBC1D15	0.00035	0.035587
MORF4L1	0.000888	0.045818
LAMTOR4	0.000546	0.039993
PSMG3	0.000677	0.041996
FCHSD1	0.000523	0.039977
SCAMP1	0.000847	0.045574
MIPEP	0.000817	0.045535

Table 1. The differential expressed genes.

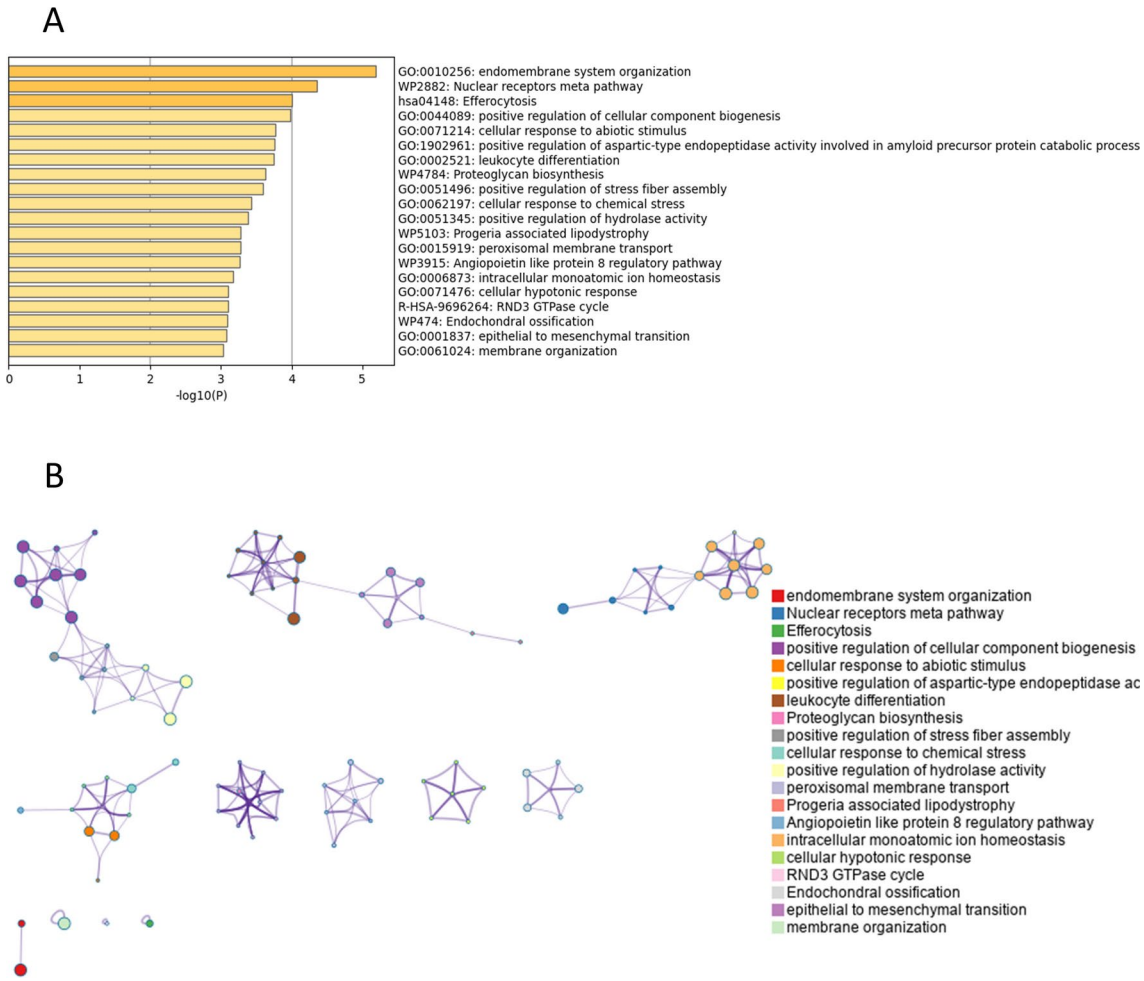

Fig. 2. Enrichment analysis of total differentially expressed genes (DEGs) by Metascape (http://metascape.org/gp/index.html#/main/step1). (**A**) Bar graph of enriched terms of total DEGs (colored by p-values). (**B**) Network of enriched terms of total DEGs, colored by cluster identity, where nodes that share the same cluster identity are typically close to each other.

the Golgi and subsequent modification, peroxisomal protein import, protein localization, peroxisome, RNA polymerase II transcribes snRNA genes, DSS1 complex, integrator complex, NRAGE signals death through JNK, cell death signaling via NRAGE, NRIF and NADE, and G alpha (12/13) signaling events. Enrichment analysis in transcription factor targets of total DEGs was performed (Table 4 and Fig. 3C) and led to the enrichment of HIF1 Q5, MTF1 Q4, PAX6 TARGET GENES, PCGF1 TARGET GENES, GTF2E2 TARGET GENES, GTF2A2

GO	Category	Description	Count	%	Log10(P)	Log10(q)
GO:0010256	GO Biological Processes	Endomembrane system organization	26	4.91	− 5.19	− 0.85
WP2882	WikiPathways	Nuclear receptors meta pathway	17	3.21	− 4.36	− 0.45
hsa04148	KEGG Pathway	Efferocytosis	11	2.08	− 4.00	− 0.37
GO:0044089	GO Biological Processes	Positive regulation of cellular component biogenesis	22	4.16	− 3.99	− 0.37
GO:0071214	GO Biological Processes	Cellular response to abiotic stimulus	16	3.02	− 3.77	− 0.37
GO:1902961	GO Biological Processes	Positive regulation of aspartic-type endopeptidase activity involved in amyloid precursor protein catabolic process	3	0.57	− 3.75	− 0.37
GO:0002521	GO Biological Processes	Leukocyte differentiation	19	3.59	− 3.75	− 0.37
WP4784	WikiPathways	Proteoglycan biosynthesis	4	0.76	− 3.64	− 0.36
GO:0051496	GO Biological Processes	Positive regulation of stress fiber assembly	6	1.13	− 3.59	− 0.36
GO:0062197	GO Biological Processes	Cellular response to chemical stress	14	2.65	− 3.44	− 0.35
GO:0051345	GO Biological Processes	Positive regulation of hydrolase activity	20	3.78	− 3.38	− 0.35
GO:0015919	GO Biological Processes	Peroxisomal membrane transport	4	0.76	− 3.28	− 0.34
WP5103	WikiPathways	Progeria associated lipodystrophy	4	0.76	− 3.28	− 0.34
WP3915	WikiPathways	Angiopoietin like protein 8 regulatory pathway	9	1.70	− 3.27	− 0.34
GO:0006873	GO Biological Processes	Intracellular monoatomic ion homeostasis	18	3.40	− 3.17	− 0.27
GO:0071476	GO Biological Processes	Cellular hypotonic response	3	0.57	− 3.10	− 0.27
R-HSA-9696264	Reactome Gene Sets	RND3 GTPase cycle	5	0.95	− 3.10	− 0.27
WP474	WikiPathways	Endochondral ossification	6	1.13	− 3.09	− 0.27
GO:0001837	GO Biological Processes	Epithelial to mesenchymal transition	7	1.32	− 3.08	− 0.27
GO:0061024	GO Biological Processes	Membrane organization	26	4.91	− 3.03	− 0.27

Table 2. Pathway and process enrichment analysis of total differentially expressed genes (Metascape, Access 2023.12.15).

MCODE	GO	Description	Log10(P)
MCODE_1	R-HSA-72766	Translation	− 14.0
MCODE_1	R-HSA-156842	Eukaryotic Translation Elongation	− 12.5
MCODE_1	R-HSA-975956	Nonsense Mediated Decay (NMD) independent of the Exon Junction Complex (EJC)	− 12.4
MCODE_2	R-HSA-3214858	RMTs methylate histone arginines	− 8.5
MCODE_2	R-HSA-9645723	Diseases of programmed cell death	− 8.0
MCODE_2	GO:0070828	Heterochromatin organization	− 7.8
MCODE_3	R-HSA-432722	Golgi Associated Vesicle Biogenesis	− 13.7
MCODE_3	R-HSA-199992	Trans-Golgi Network Vesicle Budding	− 13.2
MCODE_3	R-HSA-199991	Membrane Trafficking	− 8.4
MCODE_4	R-HSA-6807878	COPI-mediated anterograde transport	− 12.4
MCODE_4	R-HSA-199977	ER to Golgi Anterograde Transport	− 11.5
MCODE_4	R-HSA-948021	Transport to the Golgi and subsequent modification	− 11.1
MCODE_5	R-HSA-9033241	Peroxisomal protein import	− 10.8
MCODE_5	R-HSA-9609507	Protein localization	− 9.1
MCODE_5	hsa04146	Peroxisome	− 7.1
MCODE_6	R-HSA-6807505	RNA polymerase II transcribes snRNA genes	− 10.5
MCODE_6	CORUM:1154	DSS1 complex	− 9.7
MCODE_6	CORUM:1153	Integrator complex	− 9.7
MCODE_9	R-HSA-193648	NRAGE signals death through JNK	− 8.2
MCODE_9	R-HSA-204998	Cell death signalling via NRAGE, NRIF and NADE	− 7.8
MCODE_9	R-HSA-416482	G alpha (12/13) signalling events	− 7.8

Table 3. Protein–protein interaction enrichment analysis of total differentially expressed genes (Metascape, Access 2023.12.15).

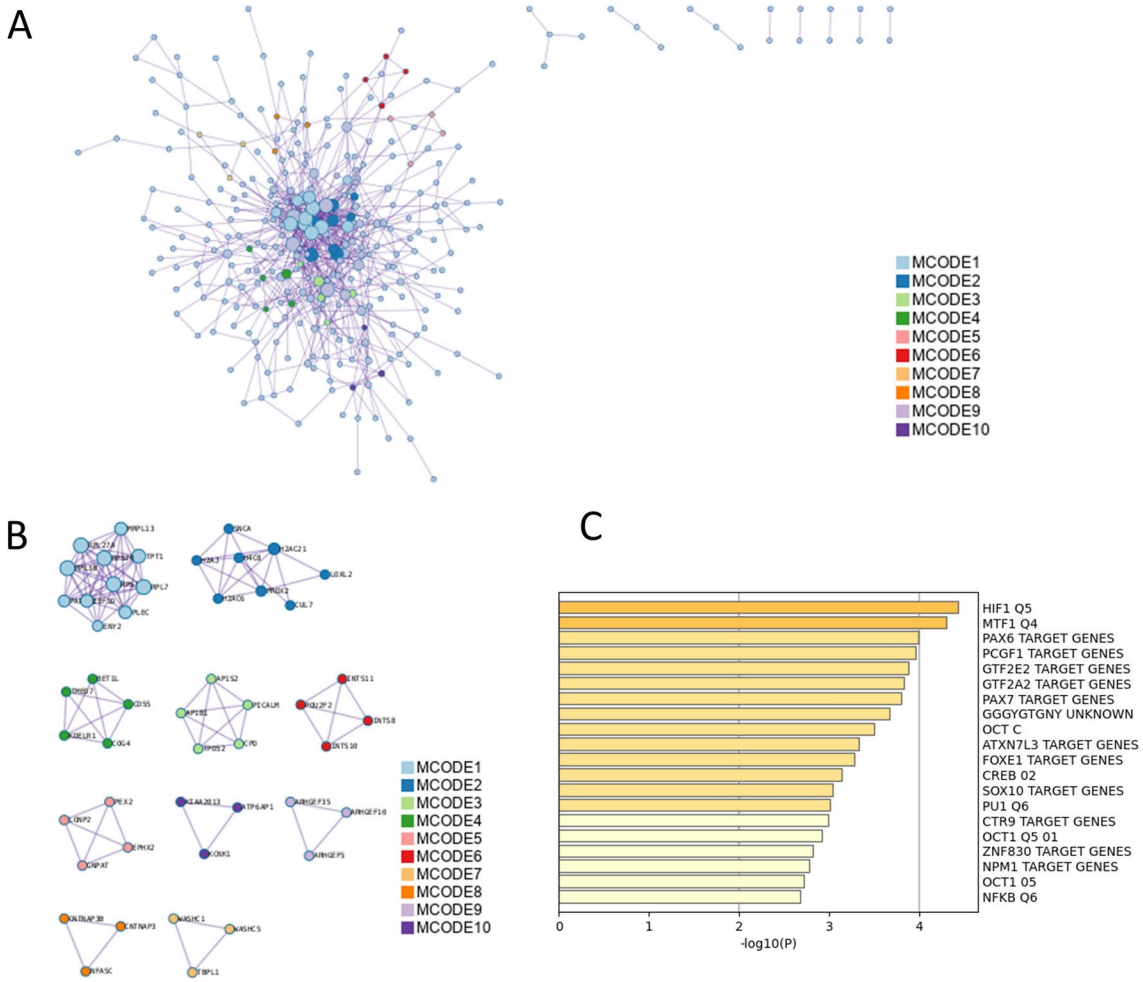

Fig. 3. Protein–protein interaction (PPI) enrichment analysis of total differentially expressed genes (DEGs). (**A**) PPI interaction network of total DEGs. MCODE algorithm was applied to clustered enrichment ontology terms to identify neighborhoods where proteins are densely connected. Each MCODE network is assigned a unique color. (**B**) PPI MCODE component associated with total DEGs. GO enrichment analysis was applied to each MCODE network to assign "meanings" to the network component. (**C**) Summary of enrichment analysis in transcription factor targets of total differentially expressed genes.

TARGET GENES, PAX7 TARGET GENES, GGGYGTGNY UNKNOWN, OCT C, ATXN7L3 TARGET GENES, FOXE1 TARGET GENES, CREB 02, SOX10 TARGET GENES and NFKB Q6.

GO functional and KEGG pathway analyses of DEGs

Both GO functional and KEGG pathway analyses of DEGs were performed using ShinyGo 0.80 and STRING database. In terms of Reactome, the DEGs were mainly enriched in pathways involved in RUNX2, FGFR, YAP1- and TAZ-stimulated gene expression, and cell cycle pathway (Fig. 4A), In terms of KEGG pathways (www.kegg.jp/kegg/kegg1.html), the DEGs were mainly enriched in pathways involved in Hippo signaling pathway, cell cycle, p53 signaling pathway, TGF-β signaling pathway, regulation of actin cytoskeleton and HIF1 signaling pathway (Fig. 4B and 4C). For GO MF analysis, the DEGs were mainly enriched in histone deacetylase activity, FGFR binding, CDK regulator activity, growth factor receptor binding and transcription factor binding (Fig. 4D and 4E). The GO analysis showed that the DEGs were significantly involved in cellular components, such as SMAD protein complex, transcription regulator complex centrosome, and nucleoplasm (Fig. 4F and 4G).

Enrichment analysis of up-regulated differentially expressed genes

Pathway and process enrichment analysis of up-regulated DEGs is presented in Table 5, Fig. 5. Functional enrichment analysis with Metascape showed that up-regulated DEGs in old corneal endothelial cells compared to young corneal endothelial cells were significantly enriched in transition metal ion transport, inorganic ion transmembrane transport, glycoprotein biosynthetic process, transport to the Golgi and subsequent modification, positive regulation of Wnt signaling pathway, extracellular matrix organization and efferocytosis.

PPI enrichment analysis of up-regulated DEGs were shown in Table 6 and Fig. 6. It led to the enrichment of RMTs methylate histone arginines, diseases of programmed cell death, transcriptional regulation by small

GO	Description	Count	%	Log10(p)	Log10(q)
M5320	HIF1 Q5	15	2.80	− 4.40	− 1.10
M2463	MTF1 Q4	15	2.80	− 4.30	− 1.10
M40719	PAX6 TARGET GENES	29	5.50	− 4.00	− 0.97
M30115	PCGF1 TARGET GENES	23	4.30	− 4.00	− 0.96
M29984	GTF2E2 TARGET GENES	19	3.60	− 3.90	− 0.92
M40742	GTF2A2 TARGET GENES	22	4.20	− 3.80	− 0.91
M30110	PAX7 TARGET GENES	27	5.10	− 3.80	− 0.90
M9645	GGGYGTGNY UNKNOWN	26	4.90	− 3.70	− 0.82
M4238	OCT C	14	2.60	− 3.50	− 0.72
M40770	ATXN7L3 TARGET GENES	14	2.60	− 3.30	− 0.64
M29968	FOXE1 TARGET GENES	26	4.90	− 3.30	− 0.61
M6342	CREB 02	13	2.50	− 3.10	− 0.54
M30173	SOX10 TARGET GENES	14	2.60	− 3.00	− 0.48
M14376	PU1 Q6	12	2.30	− 3.00	− 0.46
M29934	CTR9 TARGET GENES	6	1.10	− 3.00	− 0.45
M9638	OCT1 Q5 01	13	2.50	− 2.90	− 0.44
M30396	ZNF830 TARGET GENES	13	2.50	− 2.80	− 0.40
M34465	NPM1 TARGET GENES	15	2.80	− 2.80	− 0.40
M5708	OCT1 05	12	2.30	− 2.70	− 0.37
M11921	NFKB Q6	12	2.30	− 2.70	− 0.36

Table 4. Summary of enrichment analysis in transcription factor targets of total differentially expressed genes (Metascape, Access 2023.12.15).

RNAs, inorganic cation transmembrane transport, monoatomic cation transmembrane transport, inorganic ion transmembrane transport, Golgi associated vesicle biogenesis, trans-Golgi network vesicle budding, membrane trafficking, activated point mutants of FGFR2, phospholipase C-mediated cascade FGFR2 and FGFR2 ligand binding and activation. Enrichment analysis in transcription factor targets of up-regulated DEGs was performed (Table 7 and Fig. 6C). It showed the enrichment of HIF1 Q5, SOX10 TARGET GENES, PAX6 TARGET GENES, SRCAP TARGET GENES, CDPCR3 01, OCT1 05, NFKB Q6 and GABP B.

Enrichment analysis of down-regulated differentially expressed genes

Pathway and process enrichment analysis of down-regulated DEGs was shown in Table 8 and Fig. 7. Functional enrichment analysis with Metascape showed that down-regulated DEGs in old corneal endothelial cells compared to young corneal endothelial cells were significantly enriched in Golgi organization, eukaryotic translation initiation, integrator complex, Hippo YAP signaling, positive regulation of cellular component biogenesis, response to virus, Warburg effect modulated by deubiquitinating enzymes and their substrates, negative regulation of stem cell population maintenance, DNA metabolic process, response to starvation, secretory granule organization, positive regulation of hydrolase activity, cellular response to ionizing radiation, regulation of plasma membrane bounded cell projection organization, focal adhesion PI3K Akt mTOR signaling pathway, negative regulation of protein secretion and regulation of carbohydrate metabolic process.

PPI enrichment analysis of down-regulated DEGs were performed (Table 9 and Fig. 8). It led to the enrichment of eukaryotic translation elongation, translation, RNA polymerase II transcribes snRNA genes, DSS1 complex and integrator complex. Enrichment analysis in transcription factor targets of down-regulated DEGs was shown in Table 10 and Fig. 8C. It showed the enrichment of NPM1 TARGET GENES, PCGF1 TARGET GENES, SNIP1 TARGET GENES, GTF2E2 TARGET GENES, PAX7 TARGET GENES, MTF1 Q4 and CREB 02.

Discussion

Ageing has a significant effect on corneal endothelial cells, leading to reduced cell density, altered cell morphology and reduced regenerative capacity[20]. Indeed, understanding the changes that occur in corneal endothelial cells as a result of ageing is crucial to suggesting new therapeutic strategies for corneal endothelial cell regeneration. This study provides valuable insights into the effects of aging on corneal endothelial cells by identifying DEGs between young and old corneal endothelial cells. The key areas impacted by aging included metabolism, cell death, cellular component biogenesis, proteoglycan biosynthesis, and membrane transport. These results underscore the complex nature of aging on cellular functions, especially within the corneal endothelium, which plays a crucial role in maintaining corneal clarity and visual acuity through its barrier and pump functions[2]. The identification of DEGs in these specific biological processes suggests that aging lead to significant changes in cellular metabolism, potentially affecting energy production and the synthesis of vital components. Changes in cell death mechanisms, including apoptosis, may influence cell turnover and tissue health[21]. The impact on cellular component biogenesis indicates alterations in the ability to maintain and renew its structural components, essential for cellular integrity and function[22]. The findings related to proteoglycan biosynthesis are particularly

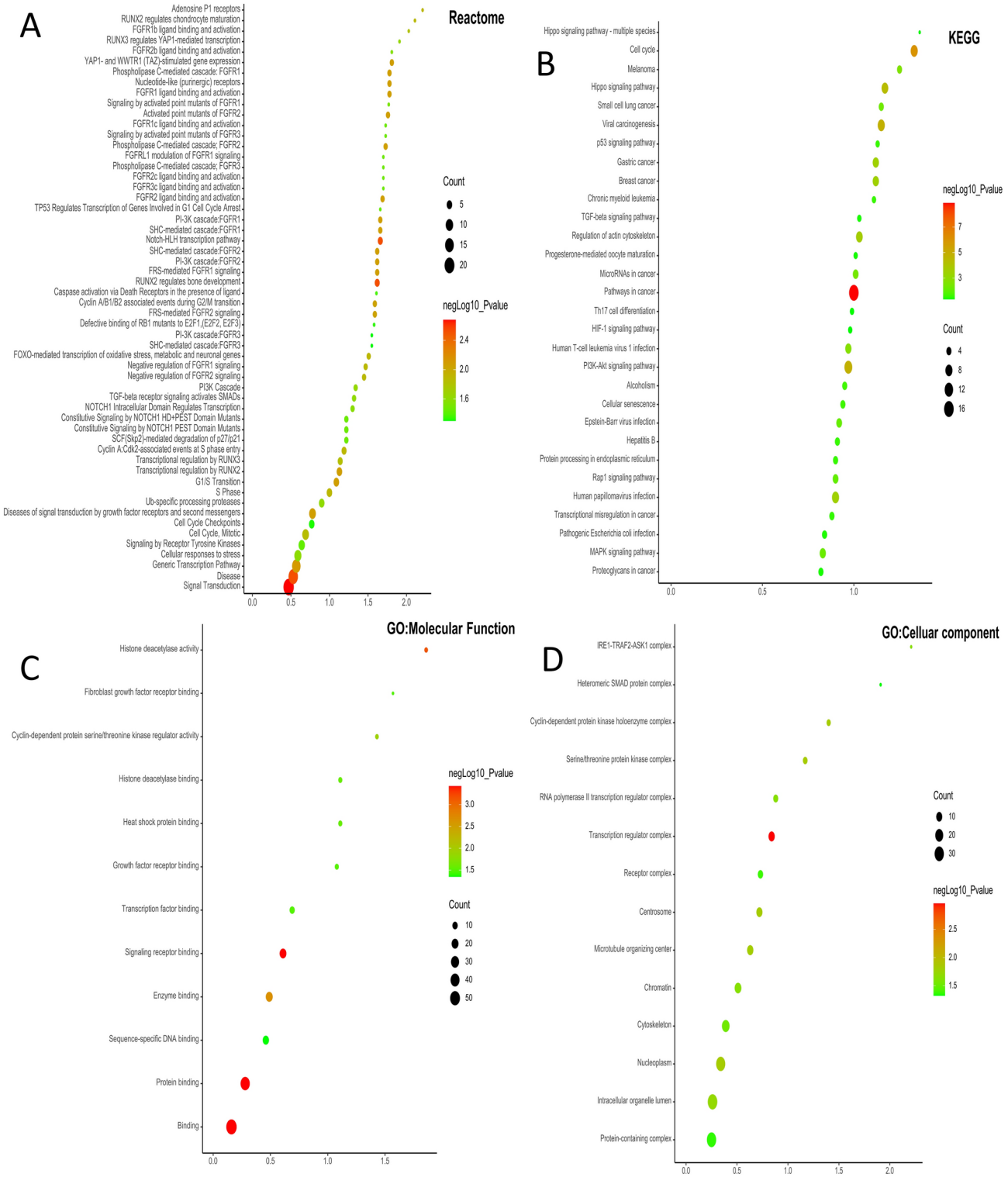

Fig. 4. Dot plots and network diagram of gene ontology using ShinyGO 0.80. Reactome (**A**), KEGG pathway analysis (www.kegg.jp/kegg/kegg1.html) (**B**), molecular functions of GO enrichment analysis (**C**), and cellular components of GO enrichment analysis (**D**) in young vs old corneal endothelial cells. Nodes represent enriched molecular functions. Size of node represents the number of genes involved in a function.

GO	Category	Description	Count	%	Log10(P)	Log10(q)
GO:0000041	GO Biological Processes	Transition metal ion transport	8	2.74	− 5.33	− 1.07
GO:0098660	GO Biological Processes	Inorganic ion transmembrane transport	21	7.19	− 5.06	− 1.07
GO:0002521	GO Biological Processes	Leukocyte differentiation	15	5.14	− 4.77	− 1.07
GO:0009101	GO Biological Processes	Glycoprotein biosynthetic process	12	4.11	− 4.75	− 1.07
GO:0060348	GO Biological Processes	Bone development	10	3.42	− 4.69	− 1.07
WP4784	WikiPathways	Proteoglycan biosynthesis	4	1.37	− 4.63	− 1.07
R-HSA-948021	Reactome Gene Sets	Transport to the Golgi and subsequent modification	9	3.08	− 4.08	− 0.88
GO:0030177	GO Biological Processes	Positive regulation of Wnt signaling pathway	8	2.74	− 4.02	− 0.88
M3008	Canonical Pathways	NABA ECM GLYCOPROTEINS	9	3.08	− 3.89	− 0.88
GO:0007435	GO Biological Processes	Salivary gland morphogenesis	4	1.37	− 3.78	− 0.88
GO:0070848	GO Biological Processes	Response to growth factor	15	5.14	− 3.76	− 0.87
GO:0030198	GO Biological Processes	Extracellular matrix organization	10	3.42	− 3.46	− 0.68
GO:0006590	GO Biological Processes	Thyroid hormone generation	3	1.03	− 3.34	− 0.66
GO:0051956	GO Biological Processes	Negative regulation of amino acid transport	3	1.03	− 3.34	− 0.66
GO:0045670	GO Biological Processes	Regulation of osteoclast differentiation	5	1.71	− 3.21	− 0.58
WP3670	WikiPathways	Interactions between LOXL4 and oxidative stress pathway	3	1.03	− 3.19	− 0.58
R-HSA-199992	Reactome Gene Sets	Trans-Golgi Network Vesicle Budding	5	1.71	− 3.18	− 0.58
GO:0050729	GO Biological Processes	Positive regulation of inflammatory response	7	2.40	− 3.13	− 0.58
GO:0051222	GO Biological Processes	Positive regulation of protein transport	9	3.08	− 3.13	− 0.58
hsa04148	KEGG Pathway	Efferocytosis	7	2.40	− 3.08	− 0.57

Table 5. Pathway and process enrichment analysis of up-regulated differentially expressed genes (Metascape, Access 2023.12.15).

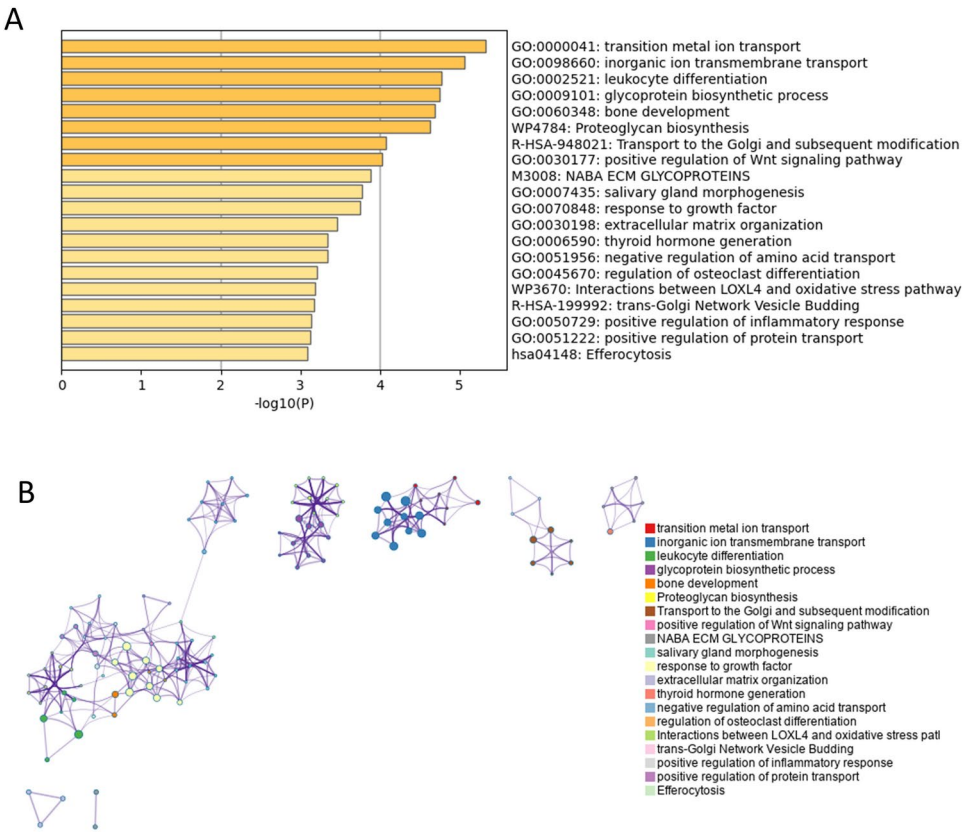

Fig. 5. Enrichment analysis of up-regulated differentially expressed genes (DEGs) by Metascape (http://metascape.org/gp/index.html#/main/step1). (**A**) Bar graph of enriched terms of the up-regulated genes (colored by p-values). (**B**) Network of enriched terms of up-regulated DEGs, colored by cluster identity, where nodes that share the same cluster identity are typically close to each other.

MCODE	GO	Description	Log10(P)
MCODE_1	R-HSA-3214858	RMTs methylate histone arginines	− 9.2
MCODE_1	R-HSA-9645723	Diseases of programmed cell death	− 8.7
MCODE_1	R-HSA-5578749	Transcriptional regulation by small RNAs	− 8.7
MCODE_2	GO:0098662	Inorganic cation transmembrane transport	− 5.6
MCODE_2	GO:0098655	Monoatomic cation transmembrane transport	− 5.5
MCODE_2	GO:0098660	Inorganic ion transmembrane transport	− 5.3
MCODE_3	R-HSA-432722	Golgi Associated Vesicle Biogenesis	− 11.0
MCODE_3	R-HSA-199992	Trans-Golgi Network Vesicle Budding	− 10.5
MCODE_3	R-HSA-199991	Membrane Trafficking	− 6.7
MCODE_4	R-HSA-2033519	Activated point mutants of FGFR2	− 9.8
MCODE_4	R-HSA-5654221	Phospholipase C-mediated cascade FGFR2	− 9.8
MCODE_4	R-HSA-190241	FGFR2 ligand binding and activation	− 9.6

Table 6. Protein–protein interaction enrichment analysis of up-regulated differentially expressed genes (Metascape, Access 2023.12.15).

relevant to the corneal endothelium, given the importance of proteoglycans in maintaining the extracellular matrix and corneal hydration[23]. Lastly, alterations in membrane transport mechanisms could affect the function of corneal endothelial cells to regulate ion and fluid balance, critical for corneal dehydration and transparency[2].

Corneal endothelial cells from old donors can proliferate more slowly than cells from young donors in the presence of fetal bovine serum and FGF, although cells from old donors can enter and complete the cell cycle[8]. Corneal endothelial cells from older donors may respond differently to EGF, media and other environmental conditions, emphasizing the need to develop treatments that consider the elderly population as a primary target for these diseases[6,9]. Protein expression of corneal endothelial cells with age has been reported. Human corneal endothelial cells from older donors show reduced expression of proteins that support important cellular functions such as metabolism, antioxidant protection, protein folding, and protein degradation[7]. Corneal endothelial cells have been reported to show heterogeneous expression of senescence markers such as *MT2A, CDKN2A* (p16)[24]. and *TAGLN*, and an increase in the senescence marker *CDKN2A* and fibrosis marker *ACTA2* with passage[25]. Additionally, it was suggested that after converting to senescent cells, there was a transition to the fibrotic cells[25]. a-SMA, COL8A1, and CD44 were suggested as fibrotic markers[26,27] and ZO-1 and CD166 were suggested as corneal endothelial cell marker and had a concomitant decrease in transition to fibrotic cells[25]. However, in this study, there was no statistical difference in corneal endothelial cell markers such as ZO-1 and CD166 and in fibrosis markers such as a-SMA, COL8A1, and CD44 between senescent and young cells.

Molecular mechanisms of aging include genomic instability, telomere attrition, epigenetic alteration, loss of proteostasis, deregulation of nutrient sensing, mitochondrial dysfunction, cellular senescence, stem cell exhaustion, and alteration of intercellular communication[28]. In this study, we found 308 up-regulated and 260 down-regulated DEGs in old corneal endothelial cells. The expression of aging-related molecules such as *TGFB1*, *FGF7*, and *IGFBP7* and functional molecules of *ATP6AP1* and *ATP1B3* increased in old corneal endothelial cells, which is consistent with the previous study evaluating mitochondria and oxidative stress in relation to aging[29–31]. The increase in expression of up-regulated genes in old corneal endothelial cells suggests two possibilities: these genes may directly contribute to the aging process, or they could be up-regulated in an attempt to compensate for the detrimental changes that accompany aging. Identifying these up-regulated DEGs provides a valuable data to target these genes for therapeutic intervention. By inhibiting the action of these genes, it may slow down or even reverse some aspects of the aging process in corneal endothelial cells. This approach could involve suppressing aging-induced transcription factor expression, which may maintain or rejuvenate the corneal endothelial cells by counteracting the molecular mechanisms that drive aging. Conversely, the genes that are down-regulated in old corneal endothelial cells may represent a decline in essential cellular functions due to aging. These could be involved in critical pathways necessary for maintaining cellular health, integrity, and function. Strategies aimed at reinforcing or supplementing these decreased DEGs could offer another therapeutic avenue to combat aging. This could involve enhancing the expression of core transcription factors that have been disrupted by aging, potentially rejuvenating the corneal endothelial cells by restoring the transcriptional regulatory networks that are essential for their function. In this study, down-regulated DEGs included proliferation genes such as *CDKL4*[32], *CDK2AP2P1*[33], *VEGFA*[34], *SINHCAF*[35], and *CCDC144A*[36] and DNA repair genes such as *PARP4*[37] *and POLG2*[38]. Proteostasis-associated genes such as *UBXN2B*[39], *PSMG3*[40], *PSD3*[41], and *ERLIN2*[42] were also down-regulated.

We found transcription factors targets which were up-regulated and down-regulated by aging. By targeting these molecular changes, either by inhibiting the action of up-regulated DEGs or enhancing the expression of down-regulated DEGs, it may be possible to develop targeted therapies that address the root causes of aging at the molecular level[43]. Such interventions could not only improve the health and function of corneal endothelial cells but also have broader implications for aging research and therapeutic development. HIF1 plays a significant role in the cellular response to hypoxia by activating signaling pathway involved in energy metabolism, angiogenesis, and other processes, which influence senescence[44–46]. MTF1, metal response element-binding transcription factor 1, regulates the expression of genes in response to heavy metals like zinc, copper, and cadmium, playing

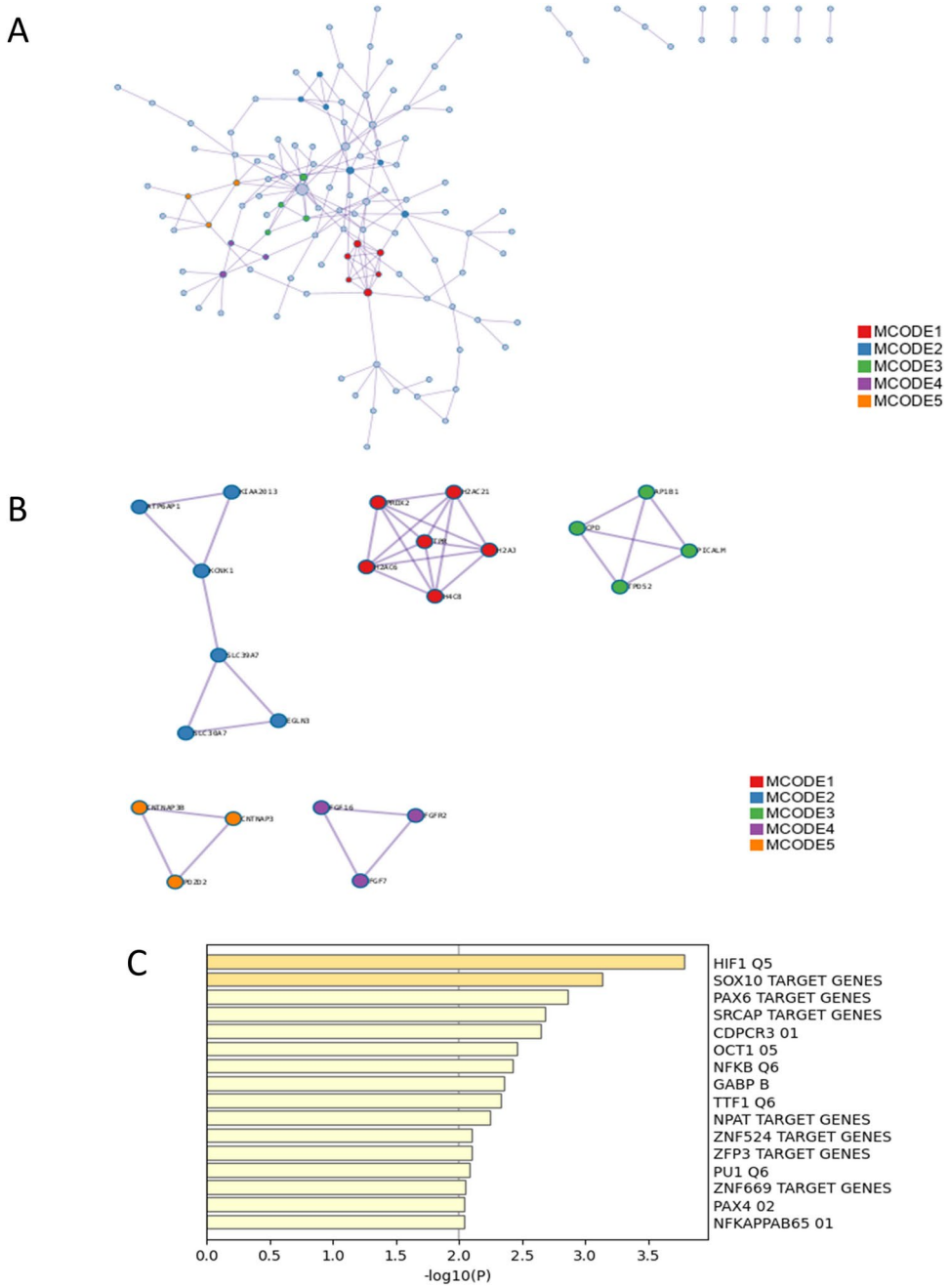

Fig. 6. Enrichment analysis in protein–protein interaction (PPI) and transcription factor targets of up-regulated differentially expressed genes (DEGs). (**A**) PPI network construction of up-regulated genes. (**B**) The essential modules identified by MCODE from the PPI network of upregulated DEGs. Ingenuity pathway analysis of genes in each sub-network to obtain the biological pathways. (**C**) Summary of enrichment analysis in transcription factor targets of up-regulated differentially expressed genes.

a crucial role in metal metabolism and detoxification processes in cells[47]. It may have an effect on senescence by regulating metallothioneins involved in metal detoxification and ROS scavenging and by regulating genes involved in detoxification and antioxidant responses[48]. NPM1, nucleophosmin 1, is a multifunctional protein and impacts on senescence by regulating p53 pathway, centrosome function, ribosome biogenesis and response to oxidative stress[49,50]. PCGF1 is a component of polycomb repressive complex 1 (PRC1), which modifies chromatin to maintain the genes in an inactive state[51]. By influencing chromatin structure and gene expression, PCGF1 affects cellular aging and senescence and is involved in stem cell renewal and differentiation[52,53]. SNIP1, smad nuclear interacting protein 1, is implicated in TGF-β signaling, the activity of p53, cellular stress responses, and cell cycle regulation[54]. Reversal and modulation of cellular senescence[55] may be useful in suppressing aging and regenerating corneal endothelial cells, in which TFs may play an important role.

GO	Description	Count	%	Log10(P)	Log10(q)
M5320	HIF1 Q5	10	3.40	− 3.80	− 0.68
M30173	SOX10 TARGET GENES	10	3.40	− 3.10	− 0.46
M40719	PAX6 TARGET GENES	17	5.80	− 2.90	− 0.35
M40790	SRCAP TARGET GENES	13	4.50	− 2.70	− 0.27
M7737	CDPCR3 01	4	1.40	− 2.70	− 0.25
M5708	OCT1 05	8	2.70	− 2.50	− 0.16
M11921	NFKB Q6	8	2.70	− 2.40	− 0.15
M6985	GABP B	8	2.70	− 2.40	− 0.11
M6331	TTF1 Q6	8	2.70	− 2.30	− 0.10
M30096	NPAT TARGET GENES	8	2.70	− 2.20	− 0.06
M30246	ZFP3 TARGET GENES	9	3.10	− 2.10	− 0.00
M30339	ZNF524 TARGET GENES	9	3.10	− 2.10	− 0.00
M14376	PU1 Q6	7	2.40	− 2.10	0.00
M30374	ZNF669 TARGET GENES	5	1.70	− 2.00	0.00
M2315	NFKAPPAB65 01	7	2.40	− 2.00	0.00
M8816	PAX4 02	7	2.40	− 2.00	0.00

Table 7. Summary of enrichment analysis in transcription factor targets of up-regulated differentially expressed genes (Metascape, Access 2023.12.15).

GO	Category	Description	Count	%	Log10(p)	Log10(q)
GO:0007030	GO Biological Processes	Golgi organization	9	3.80	− 5.67	− 1.44
R-HSA-72613	Reactome Gene Sets	Eukaryotic Translation Initiation	8	3.38	− 5.31	− 1.44
CORUM:1153	CORUM	Integrator complex	3	1.27	− 4.01	− 0.73
WP4537	WikiPathways	Hippo YAP signaling	3	1.27	− 3.19	− 0.21
GO:0044089	GO Biological Processes	Positive regulation of cellular component biogenesis	12	5.06	− 3.14	− 0.21
GO:0009615	GO Biological Processes	Response to virus	10	4.22	− 3.05	− 0.17
WP5216	WikiPathways	Warburg effect modulated by deubiquitinating enzymes and their substrates	3	1.27	− 2.97	− 0.13
GO:1902455	GO Biological Processes	Negative regulation of stem cell population maintenance	3	1.27	− 2.97	− 0.13
GO:0006259	GO Biological Processes	DNA metabolic process	15	6.33	− 2.95	− 0.13
GO:0042594	GO Biological Processes	Response to starvation	7	2.95	− 2.83	− 0.06
GO:0048515	GO Biological Processes	Spermatid differentiation	7	2.95	− 2.82	− 0.06
GO:0033363	GO Biological Processes	Secretory granule organization	4	1.69	− 2.79	− 0.06
GO:0051345	GO Biological Processes	Positive regulation of hydrolase activity	11	4.64	− 2.77	− 0.05
GO:0071479	GO Biological Processes	Cellular response to ionizing radiation	4	1.69	− 2.67	− 0.01
GO:0120035	GO Biological Processes	Regulation of plasma membrane bounded cell projection organization	13	5.49	− 2.67	− 0.01
WP3932	WikiPathways	Focal adhesion PI3K Akt mTOR signaling pathway	8	3.38	− 2.56	0.00
GO:0050709	GO Biological Processes	Negative regulation of protein secretion	4	1.69	− 2.56	0.00
GO:0006109	GO Biological Processes	Regulation of carbohydrate metabolic process	6	2.53	− 2.50	0.00
GO:0032570	GO Biological Processes	Response to progesterone	3	1.27	− 2.39	0.00
GO:0031647	GO Biological Processes	Regulation of protein stability	8	3.38	− 2.37	0.00

Table 8. Pathway and process enrichment analysis of down-regulated differentially expressed genes (Metascape, Access 2023.12.15).

In conclusion, our study has unveiled pivotal genes contributing to the aging process of corneal endothelial cells, alongside an in-depth exploration of relevant biological pathways. The identification of key genes and transcription factors involved in aging provides a solid foundation for the development of targeted therapies. These therapies may prevent the aging on corneal endothelial cells and may pave the way for innovative approaches to corneal endothelial cell rejuvenation.

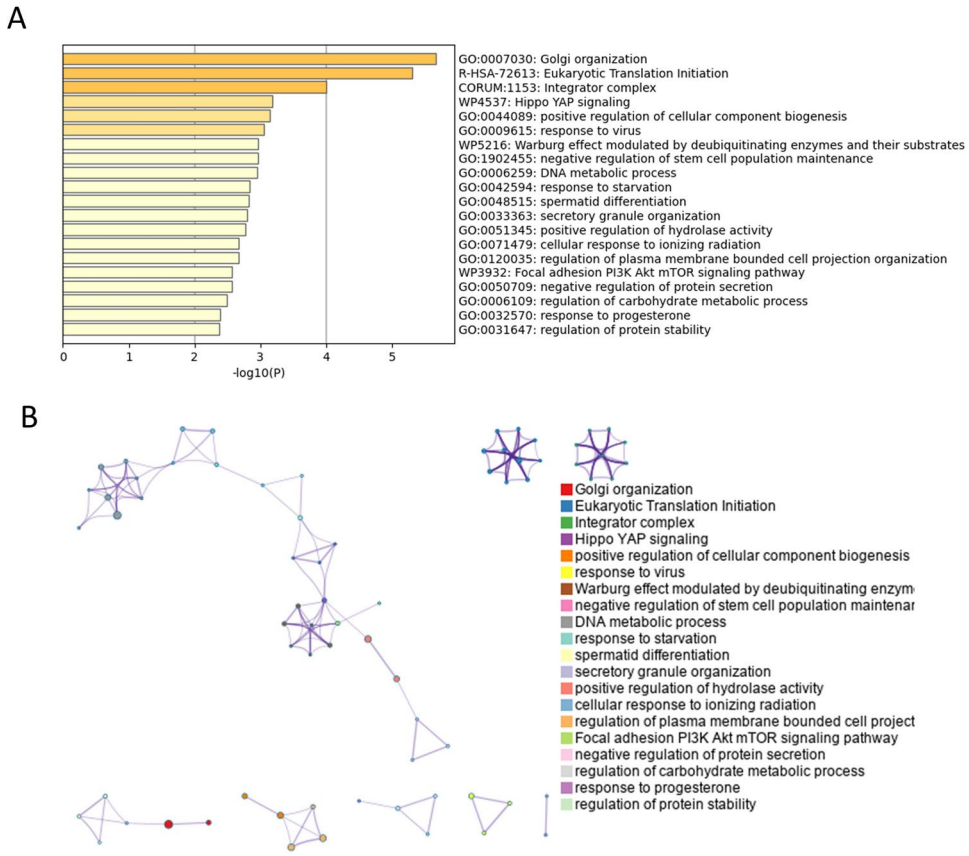

Fig. 7. Enrichment analysis of down-regulated differentially expressed genes (DEGs) by Metascape (http://metascape.org/gp/index.html#/main/step1). (**A**) Bar graph of enriched terms of the down-regulated genes (colored by p-values). (**B**) Network of enriched terms of down-regulated DEGs, colored by cluster identity, where nodes that share the same cluster identity are typically close to each other.

MCODE	GO	Description	Log10(P)
MCODE_1	R-HSA-156842	Eukaryotic Translation Elongation	− 13.2
MCODE_1	R-HSA-72766	Translation	− 12.6
MCODE_1	GO:0006412	Translation	− 11.7
MCODE_2	R-HSA-6807505	RNA polymerase II transcribes snRNA genes	− 10.5
MCODE_2	CORUM:1154	DSS1 complex	− 9.7
MCODE_2	CORUM:1153	Integrator complex	− 9.7

Table 9. Protein–protein interaction enrichment analysis of down-regulated differentially expressed genes (Metascape, Access 2023.12.15).

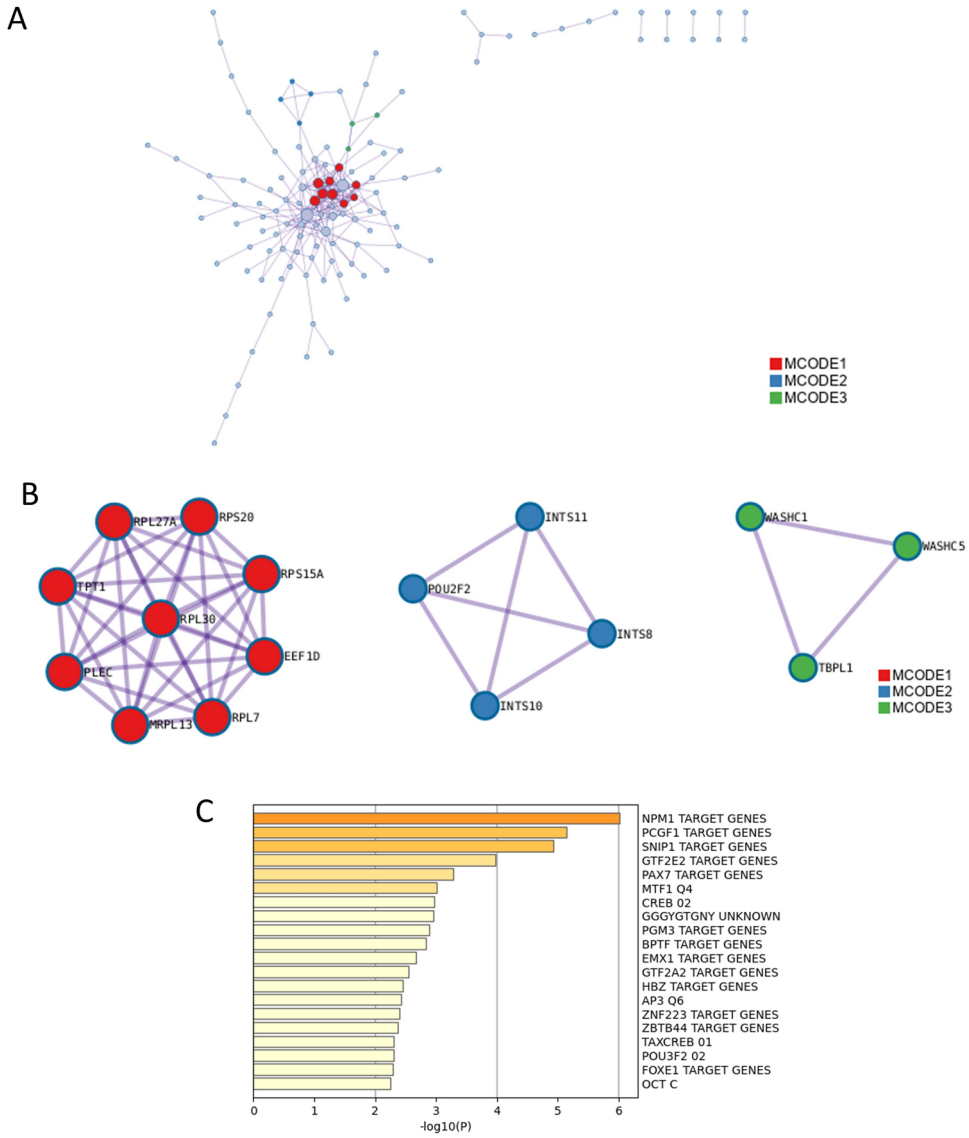

Fig. 8. Enrichment analysis in protein–protein interaction (PPI) and transcription factor targets of down-regulated differentially expressed genes (DEGs). (**A**) PPI network construction of down-regulated genes. (**B**) The essential modules identified by MCODE from the PPI network of down-regulated DEGs. Ingenuity pathway analysis of genes in each sub-network to obtain the biological pathways. (**C**) Summary of enrichment analysis in transcription factor targets of down-regulated differentially expressed genes.

GO	Description	Count	%	Log10(P)	Log10(q)
M34465	NPM1 TARGET GENES	14	5.90	− 6.00	− 1.80
M30115	PCGF1 TARGET GENES	16	6.80	− 5.10	− 1.30
M30170	SNIP1 TARGET GENES	19	8.00	− 4.90	− 1.20
M29984	GTF2E2 TARGET GENES	12	5.10	− 4.00	− 0.71
M30110	PAX7 TARGET GENES	15	6.30	− 3.30	− 0.27
M2463	MTF1 Q4	8	3.40	− 3.00	− 0.11
M6342	CREB 02	8	3.40	− 3.00	− 0.07
M9645	GGGYGTGNY UNKNOWN	14	5.90	− 3.00	− 0.07
M34464	PGM3 TARGET GENES	8	3.40	− 2.90	− 0.03
M40764	BPTF TARGET GENES	15	6.30	− 2.80	− 0.01
M29957	EMX1 TARGET GENES	7	3.00	− 2.70	0.00
M40742	GTF2A2 TARGET GENES	11	4.60	− 2.50	0.00
M40709	HBZ TARGET GENES	14	5.90	− 2.50	0.00
M498	AP3 Q6	7	3.00	− 2.40	0.00
M30281	ZNF223 TARGET GENES	8	3.40	− 2.40	0.00
M40815	ZBTB44 TARGET GENES	8	3.40	− 2.40	0.00
M5608	TAXCREB 01	5	2.10	− 2.30	0.00
M14960	POU3F2 02	7	3.00	− 2.30	0.00
M29968	FOXE1 TARGET GENES	13	5.50	− 2.30	0.00
M4238	OCT C	7	3.00	− 2.30	0.00

Table 10. Summary of enrichment analysis in transcription factor targets of down-regulated differentially expressed genes (Metascape, Access 2023.12.15).

Data availability

The data that support the findings of this study are available from the corresponding author upon reasonable request.

Received: 6 May 2024; Accepted: 5 December 2024
Published online: 28 December 2024

References

1. Feizi, S. Corneal endothelial cell dysfunction: etiologies and management. *Ther. Adv. Ophthalmol.* **10**, 2515841418815802 (2018).
2. Catala, P. et al. Approaches for corneal endothelium regenerative medicine. *Prog. Retin. Eye Res.* **87**, 100987 (2022).
3. Vercammen, H. et al. Corneal endothelial wound healing: understanding the regenerative capacity of the innermost layer of the cornea. *Transl. Res.* **248**, 111–127 (2022).
4. McHugh, D. & Gil, J. Senescence and aging: Causes, consequences, and therapeutic avenues. *J. Cell Biol.* **217**, 65–77 (2018).
5. Sheerin, A. N. et al. Characterization of cellular senescence mechanisms in human corneal endothelial cells. *Aging Cell* **11**, 234–240 (2012).
6. Zhu, C. & Joyce, N. C. Proliferative response of corneal endothelial cells from young and older donors. *Invest. Ophthalmol. Vis. Sci.* **45**, 1743–1751 (2004).
7. Zhu, C., Rawe, I. & Joyce, N. C. Differential protein expression in human corneal endothelial cells cultured from young and older donors. *Mol. Vis.* **14**, 1805–1814 (2008).
8. Senoo, T. & Joyce, N. C. Cell cycle kinetics in corneal endothelium from old and young donors. *Invest. Ophthalmol. Vis. Sci.* **41**, 660–667 (2000).
9. Merra, A., Maurizi, E. & Pellegrini, G. Impact of culture media on primary human corneal endothelial cells derived from old donors. *Exp. Eye Res.* **240**, 109815 (2024).
10. Satam, H. et al. Next-generation sequencing technology: Current trends and advancements. *Biology (Basel)* **12**, 997 (2023).
11. Srivastava, A. et al. Tissue-specific gene expression changes are associated with aging in mice. *Genomics Proteomics Bioinform.* **18**, 430–442 (2020).
12. Engler, C., Kelliher, C., Chang, S., Meng, H. & Jun, A. S. Cryopreservation and long-term culture of transformed murine corneal endothelial cells. *Graefes Arch. Clin. Exp. Ophthalmol.* **250**, 103–110 (2012).
13. Bolger, A. M., Lohse, M. & Usadel, B. Trimmomatic: a flexible trimmer for Illumina sequence data. *Bioinformatics* **30**, 2114–2120 (2014).
14. Robinson, M. D., McCarthy, D. J. & Smyth, G. K. edgeR: a Bioconductor package for differential expression analysis of digital gene expression data. *Bioinformatics* **26**, 139–140 (2010).
15. Love, M. I., Huber, W. & Anders, S. Moderated estimation of fold change and dispersion for RNA-seq data with DESeq2. *Genome Biol.* **15**, 550 (2014).
16. Pertea, M. et al. StringTie enables improved reconstruction of a transcriptome from RNA-seq reads. *Nat. Biotechnol.* **33**, 290–295 (2015).
17. Mao, X., Cai, T., Olyarchuk, J. G. & Wei, L. Automated genome annotation and pathway identification using the KEGG Orthology (KO) as a controlled vocabulary. *Bioinformatics* **21**, 3787–3793 (2005).
18. Zhou, Y. et al. Metascape provides a biologist-oriented resource for the analysis of systems-level datasets. *Nat. Commun.* **10**, 1523 (2019).
19. Zhang, X. et al. Identification of differentially expressed genes between mucinous adenocarcinoma and other adenocarcinoma of colorectal cancer using bioinformatics analysis. *J. Int. Med. Res.* **48**, 300060520949036 (2020).

20. Taurone, S. et al. Age related changes seen in human cornea in formalin fixed sections and on biomicroscopy in living subjects: A comparison. *Clin. Anat.* **33**, 245–256 (2020).
21. Park, W. et al. Diversity and complexity of cell death: a historical review. *Exp. Mol. Med.* **55**, 1573–1594 (2023).
22. Walker, C., Mojares, E. & Del Rio Hernandez, A. Role of extracellular matrix in development and cancer progression. *Int. J. Mol. Sci.* **19**, 3028 (2018).
23. Davies, Y. et al. Proteoglycans on normal and migrating human corneal endothelium. *Exp. Eye. Res.* **68**, 303–311 (1999).
24. Malavolta, M. et al. Changes in Zn homeostasis during long term culture of primary endothelial cells and effects of Zn on endothelial cell senescence. *Exp. Gerontol.* **99**, 35–45 (2017).
25. Catala, P., Groen, N., LaPointe, V. L. S. & Dickman, M. M. A single-cell RNA-seq analysis unravels the heterogeneity of primary cultured human corneal endothelial cells. *Sci. Rep.* **13**, 9361 (2023).
26. Hamuro, J. et al. Metabolic plasticity in cell state homeostasis and differentiation of cultured human corneal endothelial cells. *Invest. Ophthalmol. Vis. Sci.* **57**, 4452–4463 (2016).
27. Rao, K. B., Malathi, N., Narashiman, S. & Rajan, S. T. Evaluation of myofibroblasts by expression of alpha smooth muscle actin: a marker in fibrosis, dysplasia and carcinoma. *J. Clin. Diagn. Res.* **8**, ZC14–ZC17 (2014).
28. Guo, J. et al. Aging and aging-related diseases: from molecular mechanisms to interventions and treatments. *Signal Transduct. Target Ther.* **7**, 391 (2022).
29. Joo, H. J., Ma, D. J., Hwang, J. S. & Shin, Y. J. SIRT1 activation using CRISPR/dCas9 promotes regeneration of human corneal endothelial cells through inhibiting senescence. *Antioxidants (Basel)* **9**, 1085 (2020).
30. Tubita, A. et al. Latent-transforming growth factor beta-binding protein 1/transforming growth factor beta1 complex drives antitumoral effects upon erk5 targeting in melanoma. *Am. J. Pathol.* https://doi.org/10.1016/j.ajpath.2024.03.015 (2024).
31. He, J. et al. Single-cell transcriptomics identifies senescence-associated secretory phenotype (SASP) features of testicular aging in human. *Aging (Albany NY)* **16**, 3350–3362 (2024).
32. Baker, S. J., Poulikakos, P. I., Irie, H. Y., Parekh, S. & Reddy, E. P. CDK4: a master regulator of the cell cycle and its role in cancer. *Genes Cancer* **13**, 21–45 (2022).
33. Wong, D. T., Kim, J. J., Khalid, O., Sun, H. H. & Kim, Y. Double edge: CDK2AP1 in cell-cycle regulation and epigenetic regulation. *J. Dent. Res.* **91**, 235–241 (2012).
34. Bernatchez, P. N., Rollin, S., Soker, S. & Sirois, M. G. Relative effects of VEGF-A and VEGF-C on endothelial cell proliferation, migration and PAF synthesis: Role of neuropilin-1. *J. Cell. Biochem.* **85**, 629–639 (2002).
35. Holley, J. M. et al. Characterization of gene expression profiles in the mouse brain after 35 days of spaceflight mission. *NPJ Microgravity* **8**, 35 (2022).
36. Al-Farsi, H. et al. Discovery of new therapeutic targets in ovarian cancer through identifying significantly non-mutated genes. *J. Transl. Med.* **20**, 244 (2022).
37. Richard, I. A., Burgess, J. T., O'Byrne, K. J. & Bolderson, E. Beyond PARP1: The potential of other members of the poly (ADP-Ribose) polymerase family in DNA repair and cancer therapeutics. *Front. Cell Dev. Biol.* **9**, 801200 (2021).
38. Wojtaszek, J. L. et al. Structure-specific roles for PolG2-DNA complexes in maintenance and replication of mitochondrial DNA. *Nucleic Acids Res* **51**, 9716–9732 (2023).
39. Wrobel, L., Hoffmann, J. L., Li, X. & Rubinsztein, D. C. p37 regulates VCP/p97 shuttling and functions in the nucleus and cytosol. *Sci. Adv.* **10**, eadl6082 (2024).
40. Hsieh, Y. C. et al. Person-specific differences in ubiquitin-proteasome mediated proteostasis in human neurons. *Alzheimers Dement.* **20**, 2952–2967 (2024).
41. Hasenjager, S., Bologna, A., Essen, L. O., Spadaccini, R. & Taxis, C. C-terminal sequence stability profiling in Saccharomyces cerevisiae reveals protective protein quality control pathways. *J. Biol. Chem.* **299**, 105166 (2023).
42. Wang, J. et al. A novel autosomal dominant ERLIN2 variant activates endoplasmic reticulum stress in a Chinese HSP family. *Ann. Clin. Transl. Neurol.* **10**, 2139–2148 (2023).
43. Maldonado, E., Morales-Pison, S., Urbina, F. & Solari, A. Aging hallmarks and the role of oxidative stress. *Antioxidants (Basel)* **12**, 651 (2023).
44. Alique, M. et al. Hypoxia-inducible factor-1alpha: the master regulator of endothelial cell senescence in vascular aging. *Cells* **9**, 195 (2020).
45. Chen, S. & Sang, N. Hypoxia-inducible factor-1: A critical player in the survival strategy of stressed cells. *J. Cell. Biochem.* **117**, 267–278 (2016).
46. Gao, H. et al. Role of hypoxia in cellular senescence. *Pharmacol. Res.* **194**, 106841 (2023).
47. Olea-Flores, M. et al. ZIP11 regulates nuclear zinc homeostasis in HeLa cells and is required for proliferation and establishment of the carcinogenic phenotype. *Front. Cell. Dev. Biol.* **10**, 895433 (2022).
48. Swindell, W. R. Metallothionein and the biology of aging. *Ageing Res. Rev.* **10**, 132–145 (2011).
49. Box, J. K. et al. Nucleophosmin: from structure and function to disease development. *BMC Mol. Biol.* **17**, 19 (2016).
50. Yang, K. et al. A redox mechanism underlying nucleolar stress sensing by nucleophosmin. *Nat. Commun.* **7**, 13599 (2016).
51. Takano, J. et al. PCGF1-PRC1 links chromatin repression with DNA replication during hematopoietic cell lineage commitment. *Nat. Commun.* **13**, 7159 (2022).
52. Dupret, B., Volkel, P., Le Bourhis, X. & Angrand, P. O. The Polycomb group protein Pcgf1 is dispensable in zebrafish but involved in early growth and aging. *PLoS One* **11**, e0158700 (2016).
53. Ji, G. et al. PCGF1 promotes epigenetic activation of stemness markers and colorectal cancer stem cell enrichment. *Cell Death Dis.* **12**, 633 (2021).
54. Chen, Y., Guo, W., Guo, X., Wanqing, Q. & Yin, Z. The clinical utilization of SNIP1 and its pathophysiological mechanisms in disease. *Heliyon* **10**, e24601 (2024).
55. Rubin de Celis, M. F. & Bonner-Weir, S. Reversing and modulating cellular senescence in beta cells, a new field of opportunities to treat diabetes. *Front Endocrinol (Lausanne)* **14**, 1217729 (2023).

Author contributions

HJK, and YJS contributed to the study's conception and design. HJK and YJS conceived and designed the experiments; JSH, YKR, and YJS performed the experiments; HJK,YJS, JHS, and YL analyzed the data; JSH, JHS, and YJS wrote, reviewed and edited the manuscript. All authors read and approved the final manuscript.

Funding

This study was supported by the National Research Foundation (NRF) grant (NRF-2023R1A2C2002674) funded by the Korea government and Hallym University Research Fund funded by Hallym University.

Declarations

Competing interests
The authors declare no competing interests.

Additional information
Supplementary Information The online version contains supplementary material available at https://doi.org/10.1038/s41598-024-82423-6.

Correspondence and requests for materials should be addressed to Y.J.S.

Reprints and permissions information is available at www.nature.com/reprints.

Publisher's note Springer Nature remains neutral with regard to jurisdictional claims in published maps and institutional affiliations.